ACS Catalysis

pubs.acs.org/acscatalysis
Research Article

Reductive Treatment of Ga−Pt-Supported Catalytically Active Liquid Metal Solutions (SCALMS) for Propane Dehydrogenation

Nnamdi Madubuko, Tzung-En Hsieh, Nora Vorlaufer, Simon Carl, Julien Steffen, Andreas Mölkner, Nicola Taccardi,* Johannes Frisch, Regan G. Wilks, Johannes Will, Marco Haumann, Andreas Görling, Erdmann Spiecker, Peter Felfer, Marcus Bär, and Peter Wasserscheid*

Cite This: ACS Catal. 2025, 15, 12436−12449

Read Online

ACCESS | Metrics & More | Article Recommendations | Supporting Information

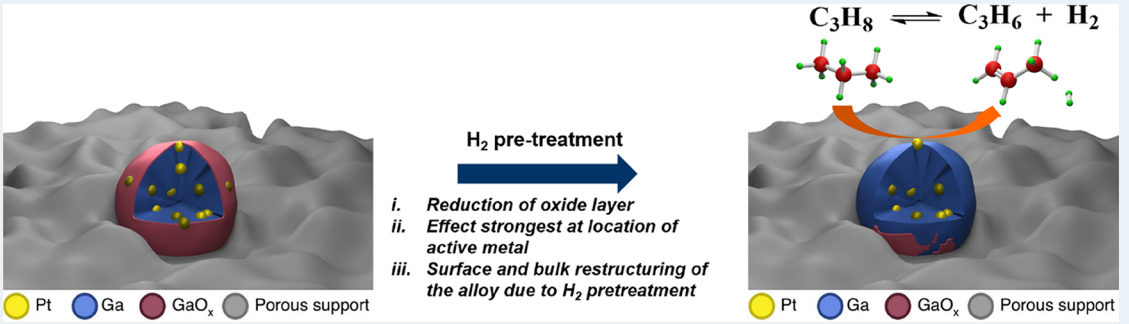

ABSTRACT: A comprehensive investigation of the impact of hydrogen (H_2) pretreatments on Ga−Pt supported catalytic active liquid metal solution (SCALMS) for propane dehydrogenation (PDH) is reported. Our approach bridges from model system investigations to real-world catalytic systems, which are tested in continuously operating PDH reactors. The microscopic and spectroscopic findings on model Ga−Pt systems suggest changes in the electronic structure and surface chemistry during SCALMS sample oxidation and H_2 pretreatment, indicating potential modifications of the active sites involved in PDH. H_2 pretreatments of technical Ga−Pt SCALMS prepared by ultrasonication (US) led to significantly improved activity, i.e., the conversion of propane increased from 10% for the untreated catalyst to 26% for the H_2 pretreated (5 h at 823 K) catalyst. We attribute this enhanced activity to the removal of a gallium oxide (GaO_x) shell, as confirmed by synchrotron-based in situ X-ray photoelectron spectroscopy (XPS) as well as in situ transmission electron microscopy (TEM) investigations of Ga−Pt model alloys. These findings are supported by density functional theory (DFT) and machine learned force field (ML-FF) calculations. Increasing the temperature of the H_2 treatment to 923 K reduced the deactivation rate of the catalyst to as low as 0.01 h^{-1}, which is 3 times more stable than what was observed for the untreated catalyst. This deactivation is ascribed to bulk restructuring of the alloy, leading to the formation of less active Pt species as confirmed by spectroscopic and microscopic analysis. Our work not only elucidates the fundamental properties, i.e., typology, electronic structure, and reactivity, of isolated Pt atoms in Ga−Pt SCALMS but also proposes underlying mechanisms for the activation and deactivation of PDH catalysts.

KEYWORDS: *propane dehydrogenation, liquid metals, SCALMS, gallium, platinum, H_2 pretreatment*

INTRODUCTION

Selective propane dehydrogenation (PDH) is an industrially relevant process for producing propylene, which is a key feedstock for the polymer and petrochemical industries. While this reaction has been commercialized, current catalysts suffer from deactivation due to coking, sintering, or poisoning of the active sites.[1−3] Thus, several strategies are currently under investigation to overcome some of these issues by the development of better catalytic materials.[1] In particular, bimetallic GaPt catalysts on silica have been demonstrated to be effective materials for this process, where the special dynamic that is established at the interphase propane/GaPt particles plays a key role in yielding the observed stability and selectivity.[4,5]

Recently, we have proposed supported catalytically active liquid metal solutions (SCALMS) as promising catalysts for PDH. In SCALMS, atomically dispersed catalytically active materials (e.g., Pt) are dissolved in an excess of a low-melting

Received: February 25, 2025
Revised: May 30, 2025
Accepted: May 30, 2025
Published: July 8, 2025

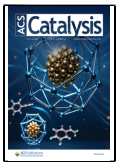

https://doi.org/10.1021/acscatal.5c01463
ACS Catal. 2025, 15, 12436−12449

metal (e.g., Ga).[6] The liquid alloy droplets synthesized by various techniques are deposited on a porous support material, e.g., alumina, silica, or mesoporous silicon carbide.[6−8] The reactants, e.g., hydrocarbon like propane, have little to no solubility in liquid gallium, and as a result, the reaction takes place at the highly dynamic interface between liquid metal and gas over the atomically dispersed active sites.[6,9] The special interfacial dynamics enhance the catalyst activity and selectivity while suppressing coke formation, which is a major challenge for the typical heterogeneous catalysts under high temperature conditions used for PDH.[7,10−12]

In this work, an easy and straightforward approach to SCALMS materials based on ultrasonication (US)[7,13] is investigated in order to address the role of the GaOx phase present after the synthesis. In fact, due to the highly oxophilic nature of Ga, a self-limiting passivating layer of gallium oxide (GaO_x) is formed, while the bulk of the Ga remains metallic.[14,15] We refer to GaO_x, rather than Ga_2O_3, to indicate that gallium oxide does not necessarily need to be stoichiometric. While this layer improves the adsorption properties of the droplets on the support, it may act as a barrier for the selective adsorption of the reactants like propane on the catalytic active sites under reaction conditions, potentially inhibiting the catalytic performance and leading to the formation of undesired side products.[10,16]

In this study, we investigate the impact of hydrogen (H_2) pretreatments on the properties of Ga−Pt SCALMS for PDH, as shown in Figure 1. We do so in a combination of model system studies and kinetic experiments in continuous PDH reactor configurations.

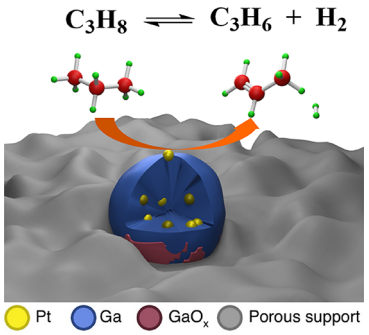

Figure 1. Schematic of Ga−Pt supported catalytically active liquid metal solution after H_2 pretreatment making the Pt active site accessible, resulting in efficient propane dehydrogenation (PDH).

Model systems of Ga−Pt alloys prepared by physical vapor deposition (PVD) on well-defined natively oxidized single-crystal silicon substrates were employed to systematically study how H_2 pretreatments affect the electronic structure, morphology, and surface chemistry of Ga−Pt alloys. Spectroscopic and microscopic techniques, such as X-ray photoelectron spectroscopy (XPS) and scanning transmission electron microscopy (STEM), were used to characterize the catalyst surfaces of these SCALMS thin-film model systems and to monitor changes in their composition and morphology in situ. Those findings were accompanied by density functional theory (DFT) calculations to shed light on the thermodynamic properties of different reaction pathways for the reduction of modeled stoichiometric Ga_2O_3 to metallic Ga using slab models and oxide nanoclusters. The dynamics of thin Ga_2O_3 layers were simulated in real-time with the help of a machine learned force field (ML-FF). These studies on model-scale SCALMS are coupled with catalytic investigations using a lab-scale continuous reactor to study the impact of H_2 pretreatments on the activity and stability of Ga−Pt SCALMS prepared by ultrasonication (US) under technically realistic PDH conditions. Applying an identical location scanning electron microscopy (SEM) and energy dispersive spectroscopy (SEM-EDS) microscopy workflow on focused-ion-beam prepared cross sections gives insights into the changes in real-world catalyst morphology by comparing (i) freshly prepared Ga−Pt SCALMS, (ii) H_2 pretreated Ga−Pt SCALMS, and (iii) the same catalyst materials after use in PDH. Our findings contribute to a comprehensive understanding of the effect of H_2 pretreatments on the properties of Ga−Pt supported SCALMS for PDH by combining insights from model system studies and from kinetic PDH studies in continuous laboratory reactors under technically realistic conditions.

RESULTS AND DISCUSSION

We employed different systems to conduct characterization and reactivity examinations. For XPS and UPS measurements, model materials prepared by PVD were obtained by the codeposition of Ga and Pt. For these specimens, the in-system approach was applied, allowing for very controlled experimental conditions. For STEM measurements, a similar approach was used using PVD for the sequential deposition of Ga−Pt model systems. For reactivity test and identical location analysis, the Ga−Pt SCALMS were synthesized via the ultrasonication method and subsequent galvanic displacement.

Characterization of the Model Ga−Pt SCALMS System in Reactive Environments. Lab-based XPS and ultraviolet photoelectron spectroscopy (UPS) investigations were conducted on a series of Ga−Pt model systems prepared by PVD with varying Pt concentrations to probe the impact of Pt isolation on the electronic structure of the Ga−Pt model catalysts before exposure to oxidative and reductive conditions. The XPS survey spectra are dominated by Ga- and Pt-related photoemission and Auger features (see Supporting Information, SI, Figure S1). As expected, with the increase of the nominal Pt content, the related XPS features also increase in intensity. The low-intensity and/or absence of O and C-related features indicate a contamination-free sample surface, documenting the advantage of the employed *in-system* approach, i.e., preparing (treating) and studying the sample in one system without the need to expose the samples to air. In the Pt 4f spectra, an approximate 1.1 eV shift to higher binding energy (BE) is observed when the Pt concentration decreases from 100 to 35 at%, indicating a drastic change in the chemical structure of the Pt atoms (Figure 2a). This can be attributed to the formation of Ga−Pt intermetallic compounds (IMCs) such as Ga_3Pt_2 or Ga_2Pt (that are thermodynamically stable at 35 at % Pt)[17] when adding Pt to Ga. Upon further diluting Pt from 35 to 11 at%, an additional +0.2 eV BE shift is observed, suggesting the formation of new Pt species. When further reducing the Pt content to 6 and 1 at%, we find indications for the dewetting of the SiO_x/Si support as demonstrated by the appearance and increase of the Si 2p photoemission line in the Ga 3p/Si 2p spectral region (Figure S2a).

Upon Pt isolation, a new spectral Pt $4f_{7/2}$ feature appears at higher BE (73.0 eV), indicating the coexistence of at least two different GaPt species in the 1 at % Pt sample (Figure 2a). The fitting of the Pt $4f_{7/2}$ peak for the 11, 6, and 1 at% Pt containing Ga−Pt sample is shown in Figure S3. Three

https://doi.org/10.1021/acscatal.5c01463
ACS Catal. 2025, 15, 12436−12449

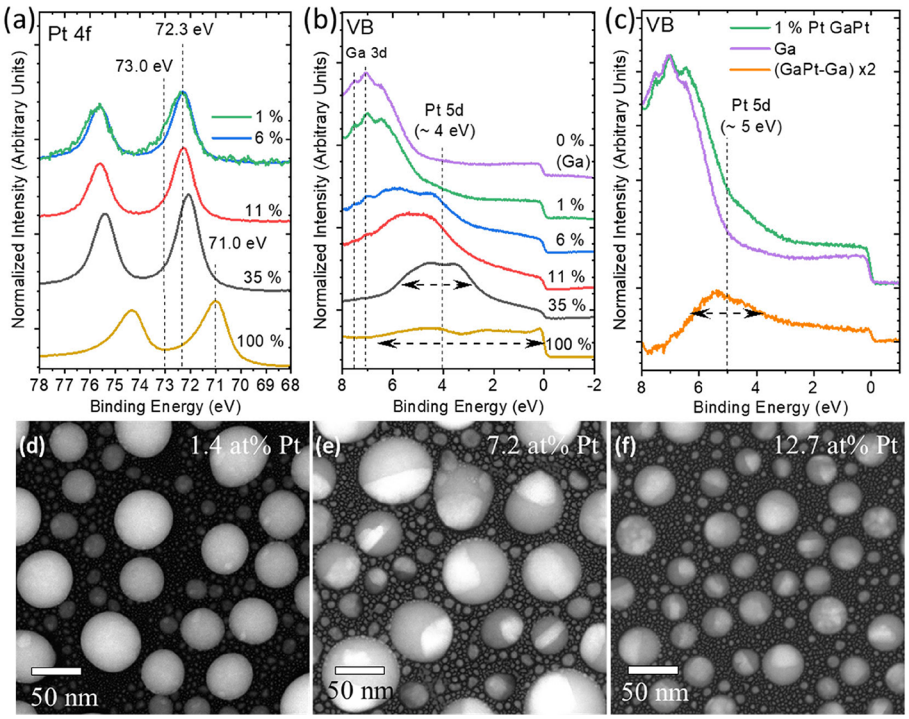

Figure 2. (a) Mg K_α (1253.56 eV) excited Pt 4f XPS spectra and (b) He II (40.8 eV) excited UPS spectra of the valence band (VB) region of the PVD-prepared codeposited Ga−Pt model alloys having Pt concentrations from 100 to 0 at% (1 at% for XPS). The stated Pt concentrations are derived based on XPS data of Pt 4f and Ga 3d core level peaks. The magnified (×2) difference spectrum for which the VB spectrum of the 0 at% Pt containing (i.e., pure Ga) sample has been subtracted from that of the Ga−Pt sample containing 1 at% Ga−Pt is shown in (c) together with the direct comparison of the initial spectra (already shown in panel b). (d−f) Representative STEM HAADF images of Ga−Pt model alloys prepared by sequential PV deposition (first Ga then Pt deposition) with 1.4 at% Pt (c), 7.2 at% Pt (d), and 12.7 at% Pt (e) all derived by STEM-EDXS, demonstrating the structural evolution of Ga−Pt SCALMS particles and formation of Ga−Pt intermetallic compounds (IMC) depending on the varying Pt content. The close-up HRTEM and HAADF STEM images of these samples are shown in Figure S4.

components, i.e., Pt_1 (at 72.3 eV BE), Pt_2 (at 73.0 eV BE), and Pt _3 (at 71.9 eV BE), are required to achieve a reasonable fit. The 73.0 eV BE feature increases with respect to the 72.3 eV BE feature when the Pt content decreases from 6 to 1 at%. According to DFT calculations of core level peak shifts for GaRh alloys[18] and GaRh IMCs,[19] the peak shift to higher BE can be regarded as an indication for the formation of Ga−Pt phases that contain either isolated or undercoordinated Pt atoms, different from metallic phases. Also, for crystalline phases, high BE peaks reflect transition metal atoms located in isolated environments, such as isolated Pt species surrounded by a Ga environment.[18] Thus, the XPS results suggest that the newly formed Pt species, most prominently observed for the 1 atom % Pt sample and resulting in additional spectral Pt $4f_{7/2}$ intensity at 73.0 eV BE, exhibits a higher degree of Pt isolation than the other probed Pt species. Note that this high BE spectral feature is unlikely to result from PtO_x since we ascribe the O 1s signal of the 6 and 1 at% Pt containing Ga−Pt sample (see Figure S2c) to the exposed SiO_x/Si support.

In Ga−Pt SCALMS, these isolated and, at elevated temperatures, highly mobile Pt atoms in the Ga matrix are considered as potential active species in the Ga−Pt catalysts.[7,13] In addition to the XPS peak shift, a narrowing of the Pt 5d-derived valence band (VB) is observed when Pt content decreases from 100 to 35 at%, suggesting that alloying Pt with Ga modifies the electronic structure of the Pt in Ga−Pt compared to metallic (100 atom %) Pt (Figure 2b). A further shift of the Pt 5d-derived VB feature from approximately 4 to 5 eV occurs when the Pt concentration decreases from 35 to 1 at % (Figure 2b,c). This shift can be considered to be an additional indication for the presence of isolated Pt sites in the Ga matrix, which might explain the higher catalytic reactivity compared to solid-state Ga−Pt phases that do not dissolve in Ga at 823 K.[17] According to previous studies related to the Newns−Anderson−Grimley adsorption model[20−22] and the work from Nørskov et. al,[23−25] the narrowed and shifted d-states may change the orbital overlap and thus the binding strength of the catalyst surface and the adsorbates, altering the catalytic performance. The composition dependence of Ga−Pt species, such as IMCs and isolated Pt atoms, is further validated by STEM measurements on PVD-deposited Ga−Pt alloys with varying Pt concentrations (Figure 2d−f). The STEM images in Z-dependent high-angle annular dark field (HAADF) contrast[26] add complementary spatially resolved information to the XPS data; however, in an oxidized state, since the samples were transferred under ambient conditions from the PVD device to the TEM. The images reveal the existence of Ga droplets of varying size (4−80 nm) generated via spontaneous dewetting of the as-deposited thin films, which also manifests in the appearance of the Si 2p core level in related XPS data in Figure S2a. The detailed particle size analysis of the 1.4 at% sample is shown in Figure S4. While investigating the particle in detail, a thin (~2−3 nm) GaO_x shell is observed on the particles (Figure S5) which is commonly observed for PVD deposited Ga−Pt thin-films exposed to ambient conditions.[27] The XPS data indicate an O deficiency; thus, the gallium oxide is labeled GaO_x rather than Ga_2O_3.[28] Whereas Ga−Pt IMCs dominate in the Ga−Pt

https://doi.org/10.1021/acscatal.5c01463
ACS Catal. 2025, 15, 12436−12449

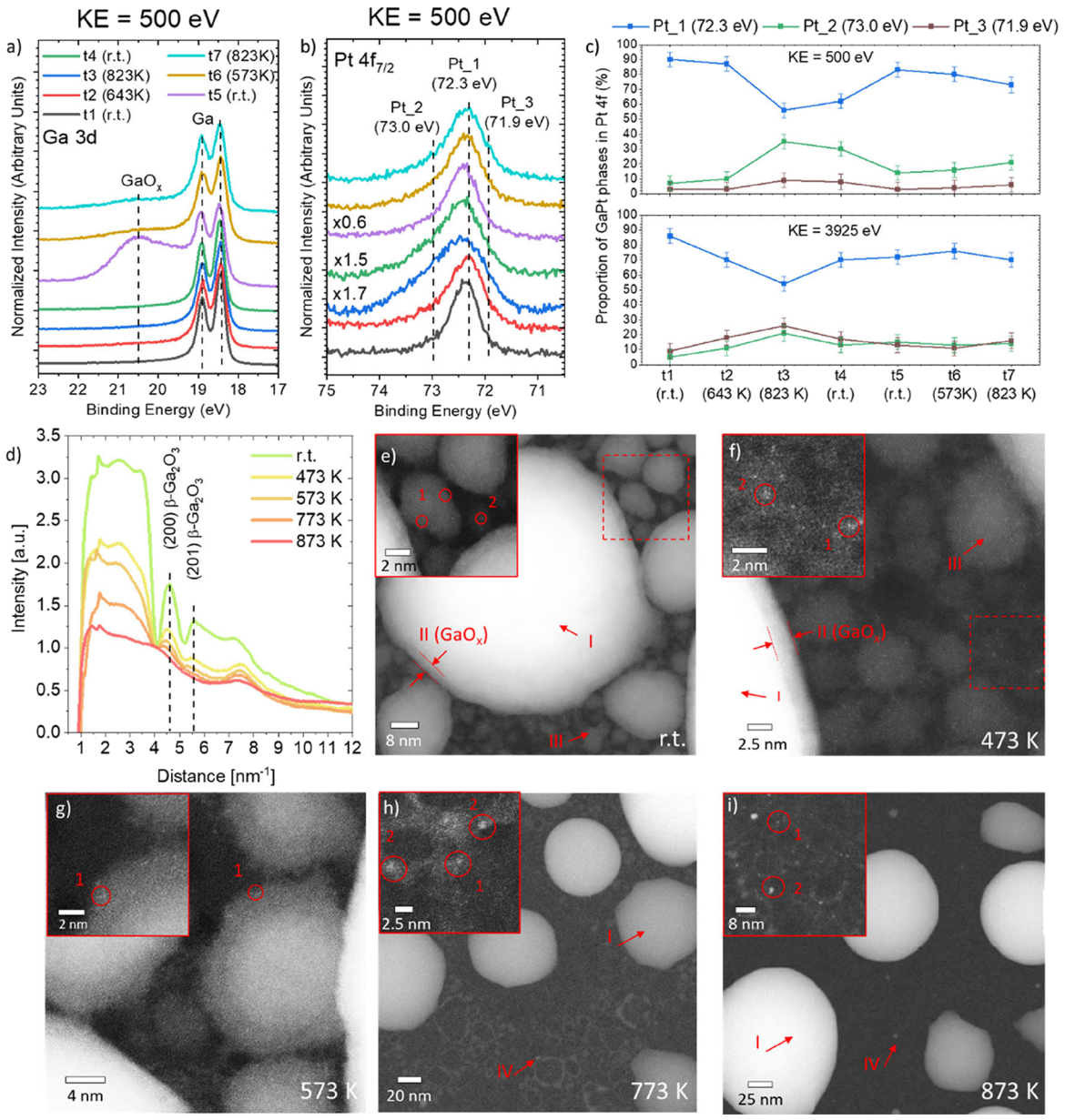

Figure 3. (a,b) Synchrotron-based Ga 3d and Pt $4f_{7/2}$ XPS spectra of a 1 at. % Pt containing Ga−Pt alloy sample before and after different treatment steps. The used photon energy was tuned such that the photoelectrons detected had the same kinetic energy, KE = 500 eV. The measurement temperatures (room temperature, r.t. −823 K) of the different treatments ([t1]−[t7]) are stated in the legend. The [t5], [t6], and [t7] treatments were performed under a reactive atmosphere of O_2, H_2 and C_3H_8, respectively. (c) Evolution of the relative abundance of the different Pt species appearing at 71.9, 72.3, and 73.0 eV required to fit the Pt $4f_{7/2}$ spectra upon performing different treatments. The upper (lower) panel depicts the surface (surface-near bulk) sensitive data based on photoelectrons detected at KE = 500 eV (KE = 3925 eV, spectra shown in Figures S8b and S12), thus having an IMFP of 1.0 nm (4.9 nm). (d) Normalized radial intensity profiles of selected area electron diffraction (SAED) patterns at selected temperatures obtained during an in situ heating TEM experiment (cf. Figure S5f–j); the SAED pattern measured at 923 K was subtracted as reference). (e–i) Selected STEM HAADF images of an in situ TEM heating experiment (starting from the oxidized state) from ambient temperature to 873 K, respectively, visualizing the evolution of large Ga droplets (I), the 2−3 nm thick oxide shell visible up to 573 K (II), heavily oxidized smaller droplets (III), and residual material after GaO_x removal at elevated temperatures (IV). Insets visualize two detected Pt species (Pt single atoms, SAs (1) and Pt rafts (2)) in their different chemical environments (support, oxide shell, and Ga core). Note that the Pt content of the TEM studied sample is 0.1 atom %, i.e., significantly different from the sample investigated with XPS.

samples containing 7.2 and 12.7 atom % Pt, their appearance is nearly extinguished for the 1.4 atom % Pt sample. Instead, Pt species as well as 1−2 nm agglomerates and single atoms, are predominantly found in the oxide shell of the Ga droplets of the 1.4 at% Pt sample (cf. Figure S5). In this context, the oxide shell apparently plays a crucial role in the segregation of Pt in close proximity to the GaO_x shell (Figure S5) as previously reported by Wittkämper et al.[17,29] and hence influences both the formation of Ga−Pt IMCs with relatively high Pt contents and the formation of isolated small Pt agglomerates. Nevertheless, both XPS and TEM demonstrate Pt isolation with decreasing Pt content in the Ga−Pt alloy, with XPS showing spectroscopic fingerprints of isolated Pt atoms in nonoxidized samples. TEM further reveals the importance of the GaO_x shell with respect to Pt segregation, agglomeration, and IMCs

https://doi.org/10.1021/acscatal.5c01463
ACS Catal. 2025, 15, 12436−12449

formation, as also recently reported for Ga−Pt SCALMS fabricated via US.[30]

In the following, we focus on the investigation of the chemical and electronic structure of Ga−Pt alloys with 1 at% Pt, i.e., with a similar composition as Ga−Pt SCALMS systems that have been described for PDH in the past.[7,12] To bridge the gap between model systems and technical operation conditions, we studied the effects of H_2 pretreatment, sample liquefaction, surface oxidation, and GaO_x removal on the properties of these Ga−Pt model alloys with XPS and TEM measurements. The conditions of treatments [t1]−[t7] are summarized in Table S1. Making use of the unique capabilities of the two-color EMIL beamline(s) at BESSY II,[31] the change of the chemical structure profile of Pt atoms is probed by both soft and hard X-ray photoelectron spectroscopy to obtain surface (electron kinetic energy, KE = 500 eV) and (near-surface) bulk (KE = 3925 eV) related information. The 1 at% Ga−Pt sample was measured at [t1] room temperature (r.t.), at [t2] 643 K (i.e., at around liquefying temperature),[17] and at [t3] 823 K (i.e., reaction temperature for PDH) subsequently. After [t2] and [t3], the spectral shape of the Ga 3d spectrum does not change significantly, indicating the presence of metallic Ga both at the surface and in the (near-surface) bulk upon liquefaction (Figures 3a and S6a, respectively). At the same time, the increased Si 2p peak intensity in the survey spectra and overlapping Ga 3p/Si 2p spectra indicate dewetting of the SiO_x/Si support (Figures S7 and S8), as it is also visualized in the STEM images depicted in Figure 3g−i showing the formation of Ga droplets as a result of dewetting upon annealing.

The same Pt $4f_{7/2}$ components at 72.3 eV BE (Pt_1), 73.0 eV BE (Pt_2), and 71.9 eV BE (Pt_3), as used for the peak analysis in Figure S3, are employed for the analysis of this XPS data (KE = 500 eV data shown in Figure S9, KE = 3925 eV data shown in S10). When performing treatments [t2] and [t3], Pt_1 remains as the major peak, but at a lower relative contribution ([t2]: 87 ± 5%; [t3]: 56 ± 5%) compared to the pristine Ga−Pt alloy model sample ([t1]: 91 ± 5%). Furthermore, the Pt $4f_{7/2}$ features at 73.0 and 71.9 eV BE become more pronounced with respect to the 72.3 eV BE feature upon sample liquefaction, suggesting an annealing (liquefaction) induced partial conversion from Pt_1 into Pt_2 and Pt_3.

According to the above discussions related to Figure 2, showing that the Pt isolation in Ga matrix can lead to the Pt $4f_{7/2}$ peak shifting to higher BE, the species Pt _2 can be attributed to Pt-depleted Ga−Pt species, e.g., Pt single atom (SA), and Pt _3 can be attributed to Pt-rich Ga−Pt species, e.g., Pt agglomerates or Pt-rich GaPt IMCs, with respect to Pt_1. As the Ga $3d_{5/2}$ peak shows dominant metallic property both at the surface and in the (near-surface) bulk region (Figures 3a, S11, and S12), these Pt phases (Pt_2 and Pt_3) are suggested to represent metallic Ga−Pt alloys with a different chemical structure rather than the formation of oxidized Pt. Interestingly, the Pt $4f_{7/2}$ peak shape somewhat differs for the surface (Figure 3b) and (near-surface) bulk sensitive measurements (Figure S6b), indicating a chemical structure profile resulting from a different depth-dependent distribution of the different Ga−Pt species in the sample. Pt_2 is mainly present at the sample surface, and Pt_3 is mainly present in the (near-surface) bulk region (Figure 3c).

Next, we discuss the subsequently performed surface oxidation experiments ([t5] in Table S1). The GaO_x feature in the surface-sensitive Ga 3d spectrum increases as expected (Figure 3a), And the respective calculated thickness of GaO_x shell is 11 ± 1 Å (cf. SI for more details on the analysis and Figure S11 and Table S2), indicating that a 1−2 monolayer thick oxide shell forms at the sample surface upon [t5]. The calculated Pt/(Ga+Pt) ratio shows the enrichment of Pt atoms at the surface during surface oxidation and GaO_x removal under reductive treatment [t6] with H_2 and [t7] with C_3H_8 (Figure S13).[32] In addition, the relative contribution of Pt_1 in the Pt $4f_{7/2}$ spectrum increases again, and a decrease in the Pt-depleted Ga−Pt species (Pt_2) is observed due to the formation of GaO_x shell as discussed above. Subsequently, upon [t6] (i.e., 573 K annealing in H_2 environment), the oxide feature of the Ga $3d_{5/2}$ spectra significantly decreases, indicating an effective surface oxide shell reduction (cf. Figures 3a and S6a). The calculated oxide shell thickness decreases to 5 ± 1 Å, which is less than the thickness of a GaO_x monolayer, indicating the possibility of exposed metallic Ga−Pt surfaces.[33,34] The latter is corroborated by the MD simulation results discussed in the following (in conjunction with Figure 4), as the distribution of oxide species is predicted to become inhomogeneous over time; i.e., the residual GaO_x on the sample surface does not form a completely covering monolayer but is presumably aggregated exposing a partially reduced Ga−

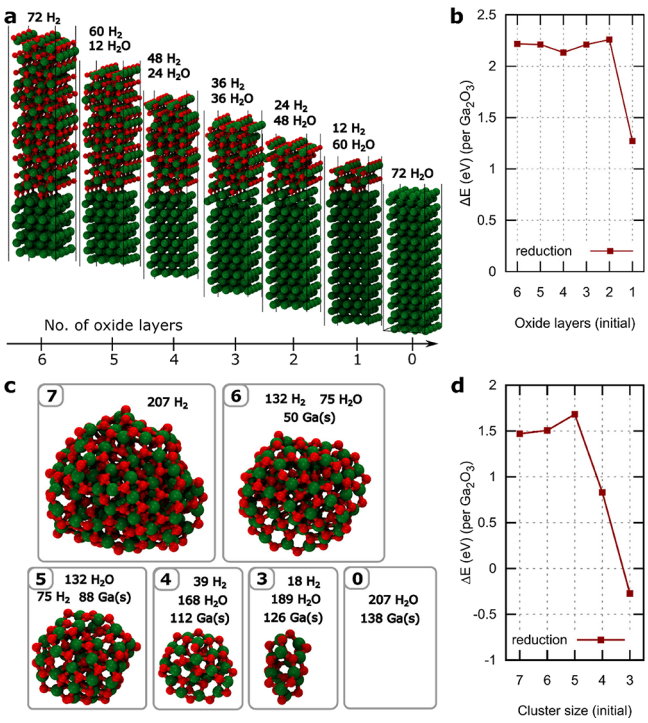

Figure 4. Static DFT investigation of the reduction of Ga_2O_3 at surfaces (a) Optimized geometries of Ga_2O_3 layers on crystalline Ga. In each step from left to right, one full oxide layer unit cell is reduced, and their Ga atoms translated to the lower surface as pure crystalline Ga. The participating gaseous species are indicated, as well. All shown structures were multiplied by 2 in the *x*- and *y*-direction (the directions parallel to the surface) for better visualization. (b) Needed energy per Ga_2O_3 formula unit to move from left to right in (a), corresponding to a successive reduction. (c) Optimized geometries of Ga_2O_3 clusters, where the gas phase species needed to balance a full reduction are added to the respective boxes. (d) Needed energy per Ga_2O_3 formula unit for the successive reduction of the clusters shown in (c).

https://doi.org/10.1021/acscatal.5c01463
ACS Catal. 2025, 15, 12436−12449

Pt surface after [t6]. GaO_x removal caused by annealing in UHV was also observed for PVD-deposited oxidized Ga and GaRh samples.[28,35] Note that the GaO_x can also form at alloy-support interfaces due to the redox reactions between Ga and SiO_x.[28] The Pt_2 contributions to the Pt $4f_{7/2}$ spectra become again more pronounced upon [t6] and [t7]. The in-depth chemical structure profiles of present Pt species as a function of all performed treatments (derived from the surface and bulk sensitive Pt $4f_{7/2}$ spectra shown in Figures S9 and S10) are summarized in Figure 3c, showing the change in relative contribution of the three Pt components to the Pt $4f_{7/2}$ spectra. The increase of Pt_2 is less pronounced upon [t7] compared to [t3]. [t7] mimics the process of Ga−Pt SCALMS preparation and activation, leading to a variation of surface Pt concentration and formation of surface GaO_x, and can influence the conversion of Pt_1 to Pt_2.

To get further insight into the evolution of the morphology and presence of species at GaO_x removal conditions at elevated temperatures, a correlative in situ TEM heating experiment of a ∼0.1 at% Pt-containing sample (as derived by XPS shown in Figure S14) was conducted. Note that the TEM sample (containing a significantly lower Pt content and on a different support SiO_x/SiN_y) is exposed to air prior to the measurements, and thus, the microscopy image in Figure 3e can best be correlated to the chemical structure demonstrated by the XPS data of the Ga−Pt sample after [t5] (Figure 3a−c). Interestingly, despite the differences in sample composition and treatments, in both the XPS and STEM HAADF experiments, we observe the removal of GaO_x and the formation of multiple Pt species upon performing different sample treatments, as discussed below. This GaO_x removal is confirmed by a detailed XPS study of a 0.1 at% Pt sample exposed to air and annealed in H_2 and UHV to bridge the different XPS and TEM sample and treatment conditions (Figure S15).

The morphological and structural evolution of the sample with an increase in temperature is summarized in Figure 3e−i. In the oxidized state at room temperature (rt) as well as up to 573 K, a few nm thick GaO_x shell surrounding the Ga-droplets is clearly visible in the STEM images (marked with II), well in line with the XPS data. At 773 K, this contrast vanishes, and the droplets become mobile on the surface. In addition, smaller Ga droplets disappear while merging with larger Ga droplets. Both observations are a clear indication of the liquid state of the system, hinting at a successful removal of the oxide shell at elevated temperatures under a reducing atmosphere, in line with the XPS study. Although the electron beam itself facilitates removal of the oxide shell, these observations hold as well for previously nonilluminated viewing areas that are not influenced by the electron beam. To validate the impression from imaging, SAED patterns have been recorded (cf. Figure S16). Overall, no sharp diffraction spots nor rings can be found, validating (i) the absence of IMCs and (ii) the amorphous or at best nanocrystalline nature of the system. Broad peaks are visible for the as-deposited sample, which fade away with increasing temperature. The ring positions match the expected ones for nanocrystalline β−Ga_2O_3. In this context, the radially averaged intensity profiles are plotted in Figure 3d documenting the fading of the β−Ga_2O_3 oxide peaks, i.e., (200) and (201) lattice fringe of β−Ga_2O_3, with increasing temperature, further supporting the successful removal of the oxide shell with increasing temperature, corroborating microscopy images, and XPS analyses.

Besides the morphological evolution of the Ga droplets and their oxide shell, STEM imaging may also elucidate what Pt species are present at rt as well as at elevated temperature. At r.t., various Pt species, e.g., Pt single atoms[36,37] and undercoordinated Pt species in the solid oxide-shell, in the solid amorphous Ga droplets, and on the SiO_x/SiN_y support are visible (c.f. insets of Figure 3e−i). This finding supports the interpretation of the XPS data, which attributes the 72.3 eV (Pt_1) and 73.0 eV (Pt_2) BE features in the Pt $4f_{7/2}$ data to undercoordinated/isolated Pt species in the Ga−Pt sample. With increasing temperature, Pt is no longer visible in the Ga core, which is likely due to the high mobility of the Pt atoms in the liquid Ga environment, resulting in a fast movement, i.e., the acquisition time for STEM imaging is too long to detect these atoms. In addition, the merging of smaller Ga particles with larger ones in the liquid state leaves the Pt-rich species as residue on the support, giving rise to Pt SAs and their agglomerates on the support. Even at elevated temperature still some isolated Pt atoms can still be found on the support as well as on residuals of the oxide shell, whereas the other initially present Pt atoms have to be dissolved in the Ga droplets (cf. inset Figure 3h,i).[37] Thus, in conclusion, we observe a higher amount of Pt dissolved in the Ga droplets and additional Pt species on the support with increasing temperature. In this context, although the direct correlation of the XPS results with the different Pt structures detected by STEM is challenging, the transformation of Pt_1 to Pt_2 and Pt_3 is likely associated with the dissolution of Pt into the Ga droplets and isolated Pt species on the support, respectively. In addition, both methods clearly reveal the removal of the oxide shell of model Ga−Pt SCALMS at elevated temperatures in reducing atmosphere, the presence of a variety of Pt species, as well as the temperature-dependent appearance/disappearance of these different Pt species. Additional in situ investigations are required to detail this picture.

Modeling the Dynamic of Ga_2O_3 Removal on Ga−Pt SCALMS. The energetics of the reduction process of β-Ga_2O_3 surfaces on α-Ga was studied on crystalline model surfaces with different numbers of oxide layers (Figure 4a,b). The systems were relaxed for zero (clean Ga surface) to 6 oxide layers (corresponding to a total oxide layer thickness of 3.7 nm), where one layer was built by one β-Ga_2O_3 unit cell, being 0.62 nm thick. The Ga atoms of reduced oxide layers were placed as new α-Ga layers on the lower side of the cell, thus conserving the total number of Ga atoms during the reduction process. The optimized structures of the seven different systems can be seen in Figure 4a.

Two different reduction mechanisms were considered in the following. First, the β-Ga_2O_3 can be fully reduced to α-Ga (here denoted as Ga(s), with the oxygen atoms completely turned into water:

$$Ga_2O_3 + 3H_2 \rightarrow 2Ga(s) + 3H_2O$$

Second, Ga can be partially reduced to gaseous Ga_2O:

$$Ga_2O_3 + 2H_2 \rightarrow Ga_2O + 2H_2O$$

In Figure 4, only the first reduction process is shown explicitly, with all involved species during each step. In Figure 4a, the successive removal of Ga_2O_3 layers is shown with the synchronous growth of metallic Ga at the lower side of the slab. All gas-phase species present at a certain point are listed as well. As can be seen in Figure 4b, each reduction step is endothermic, with roughly 2.25 eV needed per Ga_2O_3 unit for

https://doi.org/10.1021/acscatal.5c01463
ACS Catal. 2025, 15, 12436−12449

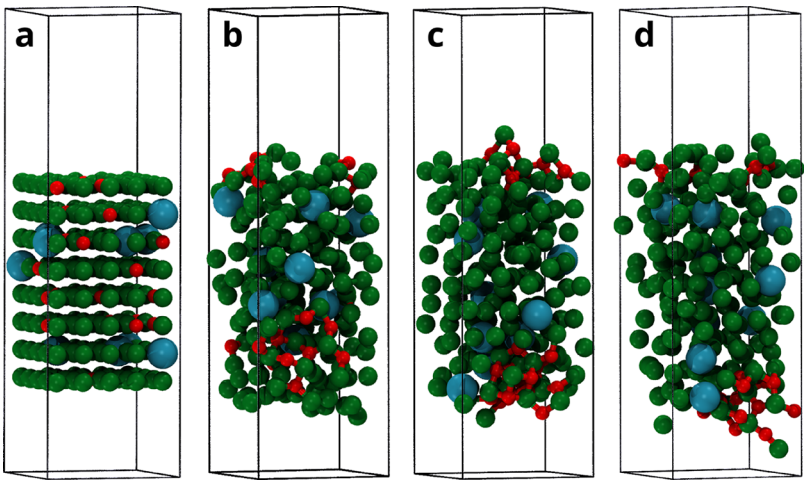

Figure 5. Screenshots of the dynamics of GaOPt with an on-the-fly machine-learned force field starting at a regular cubic grid with elements distributed randomly (a). In (b) (after 0.5 ns) some oxygen atoms have moved to the upper surface and all others merged to a cluster. In (c) (after 1.5 ns) and (d) (after 3 ns), the cluster moves to the lower surface and stays there. Ga atoms are colored green, Pt atoms colored blue and O atoms colored red.

all layers except the last one. There, the reduction energy is lower, with only 1.3 eV per Ga_2O_3 unit. It can thus be followed that very thin oxide layers can be reduced more easily than thick ones, which is in good agreement with the experimental observations in this study. The partial reduction to gaseous Ga_2O, which is not shown in Figure 4, requires almost twice as much energy per step, retaining the trend that the reduction of the last step is easier. Details can be found in Tables S3−S5.

Since the presented calculations only look at intermediate states, ignoring any reaction mechanism, it cannot be ruled out that Ga_2O might be formed as reaction intermediates and might be ejected into the gas phase, especially at higher temperatures and if no steady state is reached due to the continuous flow design of the reactor. Thermodynamically, however, the reduction to metallic Ga is clearly the preferred outcome.

In Figure 4c,d, the reduction of Ga_2O_3 clusters has been studied. In reality, reduction of oxide clusters will certainly be of some importance, since isolated Ga_2O_3 clusters will either diffuse at the SCALMS surface (see also Figure 5) or will be generated intermediately during the reduction process and associated breaking of closed oxide layers. In contrast to the surfaces, the geometries of small Ga_2O_3 clusters are not known within the literature, and of course are strongly dependent on the cluster sizes. Therefore, we obtained the investigated clusters by simulated annealing of a cubic initial structure with Ga and O atoms distributed by chance on the grid. Since a pure DFT annealing would have been by far too expensive, trajectories with on-the-fly machine-learned force fields (ML-FFs) were simulated, amounting to 0.8 ns simulation time for each cluster, after which their geometries were optimized. Details can be found in the SI. As can be seen from the Figure, the same reduction process as before has been assumed, where the metallic Ga is now modeled by multiplying the energy of a single Ga atom in a bulk unit cell. The annealing led to reasonable cluster structures of approximate spherical shape, where the bridged oxide unit cell geometry is nevertheless clearly visible. By looking at the stepwise reduction of the largest cluster to pure metallic Ga 4d, basically the same trend as for the surface can be seen. The first three steps involving large clusters result in more or less constant positive energies of 1.5 eV, indicating an endothermic process. The last two steps, however, require much less energy. The final reduction of the smallest Ga_2O_3 cluster to metallic Ga is an exothermic process. It can thus be concluded that smaller oxide clusters are more easily reducible than larger oxide clusters. The partial reduction to Ga_2O also requires much more energy, roughly a factor of 2 more (see Tables S3−S5). Further, by comparing the absolute energies in Figure 4b,d, oxide clusters are reduced more easily than oxide layers, which comes as no surprise since within our model, the oxide layers are of infinite size in two directions, thus enhancing the effect of larger structures being harder to reduce.

Next, the time-dependent surface structure of an oxidized Ga−Pt SCALMS surface was investigated. In Figure 5, four frames of the ML-FF training trajectory for a Ga−O−Pt system are shown (with 3 ns total simulation time). Frame (a) shows the initial situation of all atoms placed on a regular cubic grid with a random distribution of oxygen atoms at the surface and in the bulk. In frame (b), after 0.5 ns, some oxygen atoms have moved to the upper surface of the slab, and all others merged into a GaO_x cluster without Pt atoms. Note that an increased density of Pt atoms is observed in the vicinity of the GaO_x cluster, which can be attributed to the attractive interaction of oxide species and Pt.[32] In frames (c) and (d), the overall association of oxygen atoms does not change significantly. The large cluster in the lower part of the slab, however, has now moved to the surface of the slab, where it remains until the end of the dynamics. The oxygen atoms at the upper surface also stay there, generating an ultrathin submonolayer oxide film. The results indicate that isolated oxygen atoms prefer to move to the surface of a Ga matrix to build a thin oxide layer or to form oxide clusters. Thus, GaO_x will presumably aggregate and locate at the SCALMS surface on experimental time scales, which increases the possibility of exposing the reduced Ga−Pt surface with isolated Pt atoms (Figure S17). The advantage of a thin oxide shells for the placement of Ga droplets on a silica support can be followed from Figure S18, where it is shown that the interaction between GaPt and SiO_2 is very weak, indicating mainly physisorption, in contrast to the strong interaction of GaPt and Ga_2O_3 in Figure S17 (and presumably also between Ga_2O_3 and

https://doi.org/10.1021/acscatal.5c01463
ACS Catal. 2025, 15, 12436−12449

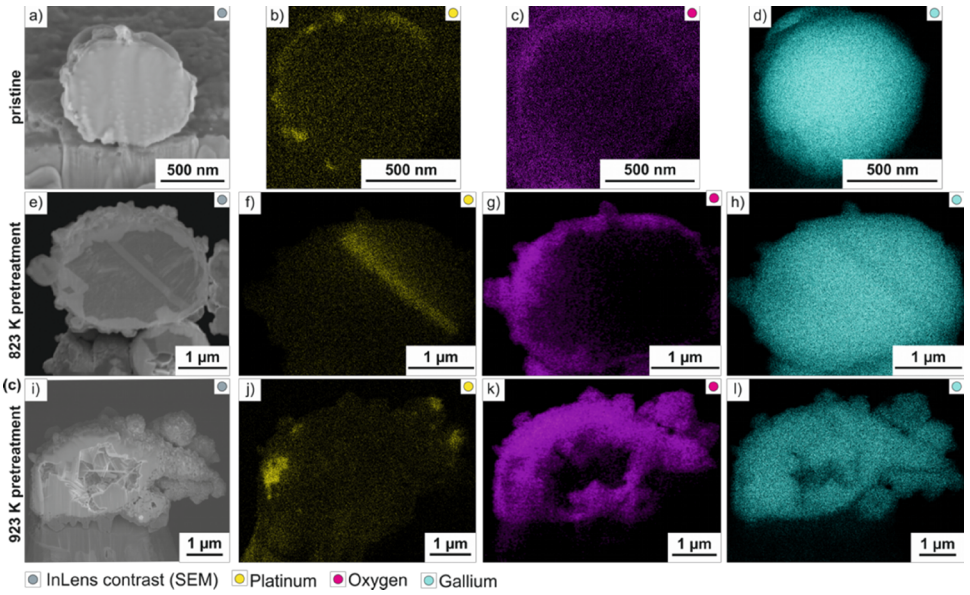

Figure 6. Scanning electron microscopy of the cryo cross sections of Ga−Pt alloys prepared by ultrasonication method showing secondary electron (SE) phase contrast and elemental map of platinum, oxygen, and gallium for (a−d) a freshly prepared pristine sample, (e−h) the Ga−Pt alloy after H_2 pretreatment at 3 h, 823 K, and (i−l) the Ga−Pt alloy after H_2 pretreatment at 3 h, 923 K.

SiO_2, due to their similar structure). Further, the accumulation of Pt atoms near the oxide layer could be observed: a small but significant Pt density maximum is visible near the Ga_2O_3 layer (Figure S17b). No such accumulation can be seen at the silica interface (Figure S18b).

Investigation of the "Technical" SCALMS System: Identical Location and Cryo Cross-Section Analysis. A microscopic identical location technique[30] was used to characterize the technical Ga−Pt SCALMS ("technical" means as applied for the catalysis) and to monitor changes in morphology induced by the H_2 pretreatment and the PDH reaction conditions. In this study, Ga−Pt alloys were prepared by ultrasonication to obtain nanometer-sized Ga droplets. Furthermore, galvanic displacement was applied to introduce the catalytically active metal Pt (see the SI for more details). The resulting alloy droplets were deposited on an oxidized silicon wafer. The prepared samples were characterized by using scanning electron microscopy and energy dispersive spectroscopy (SEM-EDS) to observe the morphology of the freshly prepared material in its pristine form. In subsequent steps, the samples were subjected to H_2 pretreatment and to PDH in our continuous reactor setup. The changes in Ga−Pt alloy structure and morphology induced under reaction conditions were investigated after each treatment step, after cooling to room temperature. Details of the identical location microscopy are described in the SI. No apparent changes were observed on the external surface of the Ga−Pt droplets due to both treatment steps (an exemplary particle showing the structure and morphology of the pristine material, after H_2 pretreatment at 823 K and after PDH at 823 K for 15 h is shown in Figure S19). However, to gain insights into the internal structure of the Ga−Pt alloy, cross-sectional analysis was performed using a focused ion beam at cryogenic specimen temperature (118 K) to avoid beam-induced melting of the Ga−Pt alloy. This "cryo cross-section" of the pristine particles in Figure 6a−d shows Pt-clusters essentially located on the outer part of the particle, as suggested in previous studies.[38] The oxygen EDS maps, as well as the SE contrast, show no areas with varying contrast or increased oxygen concentration in the inner part of the droplet. After H_2 pretreatment for 3 h, 823 K bright areas in the SE contrast match Pt-rich areas in the Pt-EDS measurement, suggesting that a Pt-rich species had formed in the particle interior. This agrees with the findings in the Ga−Pt model system elucidated by XPS and STEM (Figure 3), where evidence on the reduction of the native GaO_x shell by H_2 pretreatment has been given. This explains the dissolution of the Pt clusters initially located on the external surface of the Ga−Pt alloy (pristine material) into the bulk of metallic Ga after H_2 pretreatment (Figure 6f). The SE contrast also shows a distinct shell formed at the particles' surface that is confirmed to be an oxide layer by EDS measurement (Figure 6e−h). Note that the growth of this oxide layer occurred during sample cool-down and transfer for post-treatment investigation. In addition, the particles after PDH showed no major morphological changes in comparison to the material after H_2 pretreatment at 823 K (Figure S20). Increasing the H_2 pretreatment temperature from 823 to 923 K results in a different picture. The cryo cross-section (see Figure 6i−l) shows the emergence of a hollow structure as recently observed via identical location nano X-ray computed tomography,[30] with the Pt distributed in small aggregates close to the droplet's surface, along with an increase in the contrast of the oxygen EDS map.

By combining the identical-location and the cryo cross-section investigations, we could observe the evolution of the Pt-distribution upon H_2 pretreatment (Figure 6e−h) and PDH treatments (Figure S20). In the pristine sample, the Pt is present in concentrated islands at the outer part of the particle (Figure 6b). After the H_2 pretreatment at 823 K, Pt-rich phases formed during cooling at room temperature in the Ga bulk of the droplets. This indicates that due to the presence of Pt on the external oxide shell, the GaO_x formed around the core Ga was reduced during the pretreatment, and as a result, Pt got dissolved in the Ga-matrix, given its solubility at 823 K. In fact, after cooling the sample, the Pt recrystallizes into a rod-like

https://doi.org/10.1021/acscatal.5c01463
ACS Catal. 2025, 15, 12436−12449

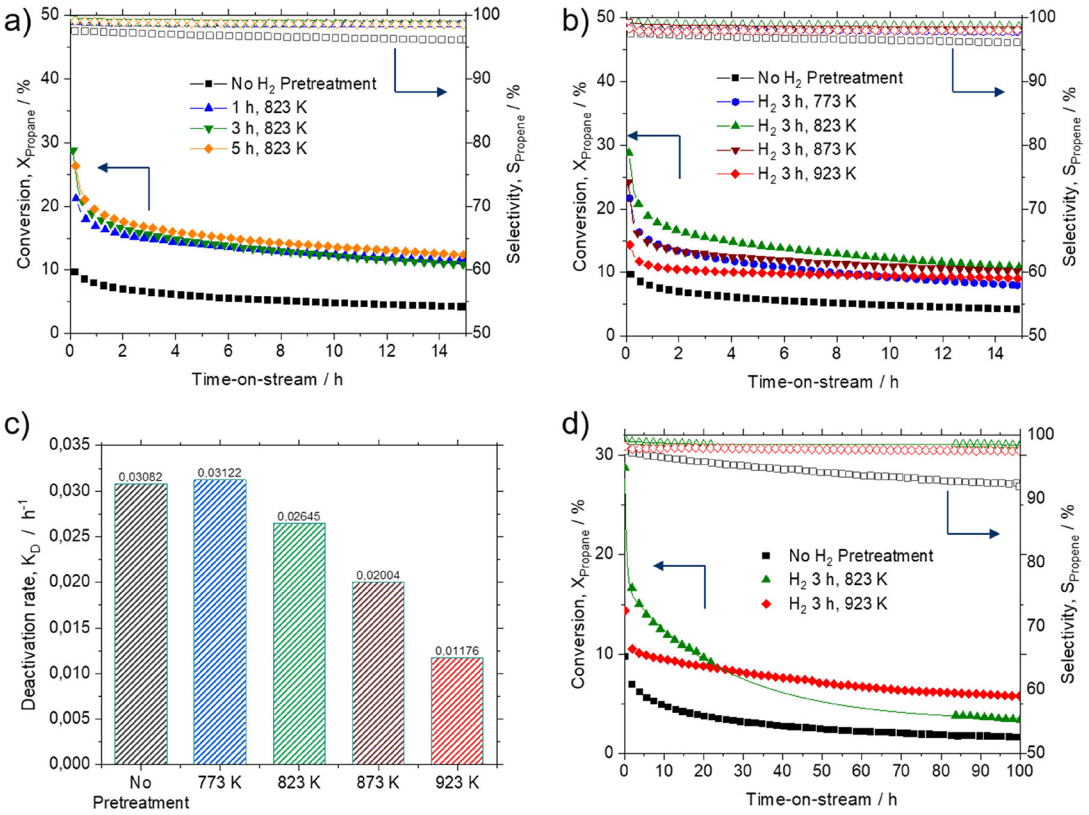

Figure 7. Catalytic performance of SiO_2 supported Ga−Pt SCALMS in propane dehydrogenation. (a) Effect of hydrogen pretreatment time on conversion (filled symbols) and selectivity (open symbols) with pretreatment at 823 K for 1 h (blue), 3 h (green), and 5 h (orange) (without H_2 pretreatment for comparison (black)). (b) Effect of hydrogen pretreatment temperature on conversion (filled symbols) and selectivity (open symbols) with pretreatment for 3 h at 773 K (blue), 823 K (green), 873 K (brown), and 923 K (red) (without H_2 pretreatment for comparison (black)). (c) Deactivation rates of various Ga−Pt SCALMS systems after 15 h time-on-stream (TOS) in PDH without H_2 pretreatment (black) and after H_2 pretreatment for 3 h at 773 K (blue), 823 K (green), 873 K (brown) and 923 K (red). (d) Effect of hydrogen pretreatment temperature on conversion (filled symbols) and selectivity (open symbols) during a long-term experiment over 100 h TOS; results without H_2 pretreatment (black) and after H_2 pretreatment for 3 h at 823 K (green) and 923 K (red) are compared (the missing points in the experiment after pretreatment at 823 K are due to failure of GC in the automated mini-plant, see SI for details. Line to guide the eyes). Catalyst bed: 1.5 g of catalyst ($Ga_{46}Pt/SiO_2$: 4.70 wt % Ga, 0.28 wt % Pt), H_2 pretreatment conditions: H_2 19.5 $mL_N\ min^{-1}$, Ar flow 78.5 $mL_N\ min^{-1}$, 0.12 mPa; PDH reaction conditions: C_3H_8 flow 8.9 $mL_N\ min^{-1}$, Ar flow 89 $mL_N\ min^{-1}$, 0.12 MPa, GHSV 3950 $mL_{gas}\ g_{Cat.bed}^{-1}\ h^{-1}$.

structure, as seen in Figures 6e and S20. The formation of two phases after cool-down to room temperature (pure Ga and a Pt-enriched phase) is also predicted by the phase diagram,[17] thus indicating the dissolution of Pt in the Ga matrix at reaction temperature. After PDH, the identical location investigation indicates that some redistribution had occurred, but the external morphology of the sample remained substantially unchanged, as depicted in Figure S19. As the pretreatment temperature was increased to 923 K, a further rearrangement of the GaPt phases and reduction of GaO_x took place, leading to new phases mainly located in proximity to the droplet surface (Figure 6i−l). Note that the formation of local GaO_x clusters is expected according to DFT calculation results (Figure 5). The inhomogeneous GaO_x induces the uneven distribution of Pt in the oxide shell since Pt has a preference to stay near GaO_x clusters, as seen in Figure 6j. Furthermore, the diffusion coefficient of Pt in a solid (i.e., Ga-oxide) is lower than in a liquid (i.e., Ga-matrix),[39] explaining the formation of small Pt phases in the 923 K pretreated and the Pt-rich phases in the 823 K pretreated particles. Furthermore, all samples showed a thicker oxide shell after thermal treatment. In this context, the observed reoxidation and thickening of the passivation layer after H_2 pretreatment (Figure 6e) results from oxygen traces coupled with the high temperature in the reactor during cool-down and shut-off of reactive gases, i.e., H_2 or propane. This was then followed by the subsequent exposure of the material to air during the transfer from the reactor to the SEM. Note that the hollow in the Ga bulk after H_2 pretreatment at 923 K could be presumably related to the oxide shell formation. Due to the reoxidation of the outer shell, the rigidity of the Ga droplets' surface is expected to increase,[40] which affects the response of the metal to the thermal contraction due to cooling. Others also observed this hollow structure and attributed it to the cracking of the oxide shell and the release of liquid Ga−Pt into the surrounding network.[30] The solubility of H_2 in Ga is known to increase linearly with temperature.[41−43] During the cool-down, the solubility of hydrogen in Ga decreases again, while the droplet cannot freely contract due to the solid oxide layer, the latter hindering also the escape of the dissolved H_2 in Ga. Consequently, the outgassing of H_2 at low temperatures can also lead to the observed voids in the Ga bulk.

Catalytic Performance of Ga−Pt SCALMS in Propane Dehydrogenation. Based on the insights generated from these detailed investigations on the structural and electronic properties of Ga−Pt alloys, a lab-scale continuous flow reactor

https://doi.org/10.1021/acscatal.5c01463
ACS Catal. 2025, 15, 12436−12449

(Figure S21) was used to study the effect of H_2 pretreatment on the performance of Ga−Pt SCALMS for the PDH. A silica (SiO_2) supported Ga−Pt SCALMS with a composition similar to that investigated in the model systems was used to study the effect of varying H_2 pretreatment time (0−5 h) and pretreatment temperature (from 773 to 923 K), as shown in Figure 7. The Ga−Pt SCALMS was prepared by a sequence of Ga ultrasonication and galvanic displacement (more details in the SI).[7,13,44] For direct comparison, equal amounts from the same batch of the Ga−Pt SCALMS were used for each experiment, with the same pretreatment gas composition, i.e., 20 vol % H_2 in argon. Similarly, the same PDH reaction conditions of 823 K, 0.12 MPa, gas hourly space velocity (GHSV) of 3950 $mL_{gas}\ g_{Cat.bed}^{-1}\ h^{-1}$ and 10 vol % propane in argon were used for each experiment. As reference experiments, the effect of H_2 pretreatment on Ga/SiO_2, Pt/SiO_2, and Ga_2O_3/SiO_2 was tested under identical conditions. In all cases, the reference materials showed significantly lower activities (Figure S22). It has been reported,[45] the interaction of GaO_x with Silica might result in the formation of an isolated Ga^{3+}/SiO_2 site that can contribute to the observed PDH activity. Nevertheless, our support variation investigation,[7] showed that materials with fundamentally different surface chemistry compared to SiO_2, i.e., Al_2O_3 and SiC, produced very active catalysts as well. Thus, although it could not be completely ruled out, it seemed unlikely that such Ga^{3+}/SiO_2 sites could play a key role in the SCALMS case. A control experiment shows that the SiO_2 support is not active for PDH under the same experimental conditions (Figure S23).

Figure 7a shows the effect of the duration of the H_2 pretreatment on the conversion and selectivity of the SiO_2-supported Ga−Pt SCALMS materials in the PDH at 823 K. The catalyst without H_2 pretreatment showed an initial conversion of 9.8% and a final conversion of 4.1% after 15 h TOS. In comparison, the catalyst pretreated with H_2 for 1 h, 823 K showed a notable enhanced catalytic performance, with the initial conversion increasing to 21.2%. In fact, as the amount of catalyst was kept constant along the experiments, this corresponded to more than a doubling in catalytic activity compared to the catalyst without H_2 pretreatment. The productivity of the catalyst without H_2 pretreatment was 170 $g_{propene}\ g_{pt}^{-1}$ over 15 h TOS, and it increased to 383 $g_{propene}\ g_{pt}^{-1}$ for the catalyst after 1 h H_2 pretreatment (Figure S25). Further increasing the H_2 treatment time to 3 h, 823 K, led to a further increase in the initial activity to 28.7%. The Ga−Pt SCALMS material pretreated with H_2 for 5 h, 823 K, showed the best catalytic performance over the 15 h TOS (initial conversion of 26.1% and final conversion of 12.5%). The increase in conversion with longer H_2 pretreatment time is attributed to the removal of the GaO_x layer on the Ga−Pt SCALMS surfaces. As shown by the XPS data, the GaO_x on the Ga−Pt model system was significantly removed when exposed to 1×10^{-9} MPa of H_2 at 573 K. The model catalyst surfaces remained oxide-free even after exposure to 1×10^{-9} MPa of propane (cf. [t7] in Figure 3a). As previously described, GaO_x forms during catalyst preparation, which behaves as a passivating layer, preventing adsorption of propane on the catalytic active sites under reaction conditions.[14,15] As a result, the catalytic performance decreases as indicated by the results without H_2 pretreatment. Furthermore, the GaO_x sites can activate both C−H and C−C bond cleavage, leading to the formation of undesired side products.[46] Accordingly, lower propene selectivity is observed for the catalyst without H_2 pretreatment. On the contrary, all catalysts pretreated with H_2 showed stable selectivity above 98%. The superior performance observed for the catalyst after H_2 pretreatment strongly suggests that under these conditions, the passivating GaO_x layer can be reduced, giving rise to improved accessibility to the highly dynamic active sites present in the SCALMS catalyst.[6,7] As shown by the calculations and modeling of the dynamics of the Ga_2O_3 layer removal in the Ga−Pt systems (vide supra), the reduction of Ga_2O_3 to metallic Ga is energetically favorable compared to the reduction of volatile Ga_2O when the sample is present in an H_2-rich atmosphere. In addition, several studies have shown that the presence of catalytically active Pt enables the Ga_2O_3 reduction process.[47−49] Further, these phenomena were also analyzed by applying in situ Raman spectroscopy to samples treated at 823 K.[50] The treatment with hydrogen caused the disappearance of bands assigned to Ga_2O_3 in the Ga−Pt SCALMS catalyst. On the other hand, blank Ga/SiO_2 materials showed a significant tendency toward coke formation, which is remarkable considering that those materials possess very low activity in PDH. Altogether, this evidence pointed out that while the reduction led to more accessible and active PtGa sites, the presence of unreduced GaOx phases may act as a coking and cracking source.

Furthermore, the effect of the H_2 pretreatment temperature on the Ga−Pt SCALMS performance was studied, as shown in Figure 7b. For all studied pretreatment temperatures, higher conversion and selectivity than for the untreated catalyst were observed. Interestingly, a change in the catalyst stability was found with increasing H_2 pretreatment temperature. H_2 pretreated for 3 h at 823 K, the catalyst showed the highest conversion of 28.7%. However, this was followed by a strong exponential decay in activity, leading to a final conversion of 10.8%.

The same behavior was observed for the catalyst after 3 h at 773 K H_2 pretreatment. This material showed an initial conversion of 21.6% and a final conversion of 14.8%. In contrast, increasing the H_2 pretreatment temperature to 873 K resulted in a catalyst with 24.1% initial conversion that dropped to a final conversion of 10.2% after 15 h TOS. A further increase of the H_2 pretreatment temperature to 923 K resulted in the most stable performance, although with a lower initial conversion of 14.3% that dropped to 9.1% after 15 h TOS. The activity profile of Ga−Pt SCALMS in PDH could be fitted with a two-phase second-order exponential (Figure S24). In general, all of the materials tested showed the same trend of a strong exponential loss in activity in a short first phase, followed by a second phase with a slow but progressive loss in activity. The catalyst with 3h H_2 pretreatment at 773 and 823 K shows deactivation profiles similar to the untreated catalyst (Figure 7c). By increasing the H_2 pretreatment temperature from 823 to 923 K, the catalyst showed a gradual increase in stability, leading to a deactivation rate of only 0.012 h^{-1}, which is 3-fold more stable than the catalyst without H_2 pretreatment. In terms of conversion, the catalyst lost only 1.8% of its activity from 1 h (conversion of 10.9%) to 15 h (conversion of 9.1%) time-on-stream. A long-term stability test over 100 h of PDH is shown in Figure 7d. Herein, we compare the most active (H_2 pretreatment for 3 h at 823 K) and the most stable (H_2 pretreatment for 3 h at 923 K) pretreated catalysts with the untreated catalyst as a benchmark. We observe that due to its higher stability, the catalyst pretreated at 923 K outperforms its counterpart pretreated at 823 K after 25 h of operation (TOS).

https://doi.org/10.1021/acscatal.5c01463
ACS Catal. 2025, 15, 12436−12449

Hence, the slightly lower initial activity for the latter catalyst is compensated over time, resulting in an overall better catalyst performance and cumulative productivity, exceeding an overall value of 1500 g of propene per gram of Pt over 100 h TOS (Figure S25). These results are in good agreement with our XPS and HRTEM findings in the Ga−Pt model systems regarding the role of post-treatments in Ga−Pt SCALMS systems (Figure 3c). While minimal improvements could be achieved in limiting the activity loss in the first deactivation phase, the catalyst stability during the second deactivation phase can be clearly improved by the H_2 pretreatment at high temperatures (Figure S24). It is worth noting that all H_2 pretreated catalysts showed stable selectivity above 98% over the entire 100 h time-on-stream, while the untreated catalyst showed a progressive decrease in selectivity from 97.5 to 92% over the same period. The main byproducts are shorter hydrocarbons resulting from propane cracking, i.e., methane and ethane. Moreover, coking was also observed.[11,50]

Our testing setup also allowed us to check whether the observed pretreatment effects are really linked to the reductive role of hydrogen (as expected from our spectroscopic, microscopic, and modeling results) or whether some effects are also only due to thermal effects. To clarify this important aspect, we subjected our SiO_2-supported Ga−Pt SCALMS catalyst material to the same pretreatment conditions, but now using Ar instead of hydrogen. In addition, we also tested pretreatment using different partial pressures of H_2 (Figure S26). The catalyst subjected to thermal pretreatment at 923 K using only Ar showed a similar activity profile to the catalyst without H_2 pretreatment. Whereas increasing the partial pressure of the pretreatment gas H_2 at 923 K led to the expected increase in conversion and catalyst stability (Figure S26). The decrease in initial conversion after H_2 pretreatment at 923 K is likely due to the increased mobility of the liquid alloy nanodroplets on the support surface, leading to coalescence and subsequent loss of the active surface. This droplet agglomeration is visualized by the particle size analysis shown in Figure S27. After operating the H_2 pretreatment and PDH at 823 K, the average particle size increased from 620 ± 99 nm to 706 ± 95 nm (Figure S27). This phenomenon has been reported for Ga−Pt model SCALMS on modified highly oriented pyrolytic graphite (HOPG), where the thermal behavior of the Ga−Pt alloy droplet was investigated in UHV.[51] Herein, a growth in Ga droplet agglomerations upon annealing with increasing temperatures was observed.[51] Furthermore, the SEM analyses on technical Ga−Pt SCALMS have also shown that under reductive conditions, the mobility of Ga is strongly increased, leading to a significant drifting of the Ga droplets, eventually inducing the phase segregation and forming Pt-depleted and Pt-rich phases (Figure 6). This aligns with the XPS and TEM results and can be a reason for the variation of catalytic reactivity and deactivation of the catalysts. Moreover, the presence of the oxidized phase may contribute to the observed deactivation as it acts as a source of coking, leading to surface fouling over long reaction times. Therefore, high-temperature treatment might result in a reduced amount of oxidized phases on the catalytic material, with consequent reduced tendency to coking. However, temperature restriction arising from alloy coalescence effects, the onset of formation of volatile Ga_2O species, and condensation of silanol groups on the silica support should be considered. In the investigated conditions, there was no hint that these phenomena might have occurred. However, at higher temperatures, these effects might be very relevant, and therefore, we have not tested H_2 pretreatment temperatures above 923 K in this study.

CONCLUSIONS

This study provides a comprehensive understanding of the effect of H_2 pretreatment on Ga−Pt SCALMS for propane dehydrogenation (PDH). The results of our in situ investigations on model systems prepared by PVD provided insights into the structure of Ga−Pt droplets, revealing the concomitant existence of at least 3 different Pt species in the liquid Ga−Pt system. These could be reasonably assigned to be single Pt atoms dissolved in Ga, Ga-rich Ga−Pt IMCs, and Pt-rich rafts, respectively. We observed changes in the surface chemistry of the catalyst by exposure to a reactive environment, indicating potential modifications of the active sites involved in propane dehydrogenation due to H_2 pretreatment. Identical location measurements on Ga−Pt droplets prepared by ultrasonication and galvanic displacement confirmed the high dynamics of these systems, as bulk restructuring of the alloy under pretreatment conditions leads to the formation of new Ga−Pt IMCs depending on the condition of H_2 pretreatment and reaction with propane. DFT and molecular dynamics calculations have shown that direct reduction from Ga_2O_3 to metallic Ga is the most thermodynamically favored reaction, with thin oxide layers and small oxide clusters being easier to reduce in the presence of Pt. The latter could be facilitated by the fact that both the Pt and the oxygen tend to move toward the surface of the liquid metallic droplets, as indicated by the time-averaged samplings of the GaPt-Ga_2O_3 interface. Finally, the impact of H_2 pretreatment on Ga−Pt SCALMS prepared by the ultrasonication method and galvanic displacement resulted in a significant improvement in catalyst activity. An over 100% increase of the initial PDH activity was found after a H_2 pretreatment at 823 K for 5 h, prior to the propane dehydrogenation reaction (10% conversion for a catalyst without H_2 pretreatment vs 26% conversion for the pretreated catalyst). The reason for this increase in activity could be attributed to the removal of the GaO_x layer from the alloy droplets/nanoparticles, as confirmed by XPS measurements. Furthermore, a significantly improved catalyst stability was obtained for a harsher H_2 pretreatment with temperatures up to 923 K. As demonstrated in a 100 h time-on-stream experiment, a so-pretreated catalyst showed a very low deactivation rate of 0.01 h^{-1}, which is 3 times lower than found for the respective catalyst without any pretreatment. We anticipate that the insights presented here will help to develop Pt-based SCALMS materials for valuable catalyst systems for industrial alkane dehydrogenation applications.

ASSOCIATED CONTENT

Data Availability Statement

The data set of XPS spectra present in this manuscript and Supporting Information is accessible with following Zenodo link: 10.5281/zenodo.12773270.

Supporting Information

The Supporting Information is available free of charge at https://pubs.acs.org/doi/10.1021/acscatal.5c01463.

Detailed description of PVD, XPS/UPS, TEM, SEM, MD, and DFT methods, catalyst preparation, catalyst testing rig, and procedure (PDF)

https://doi.org/10.1021/acscatal.5c01463
ACS Catal. 2025, 15, 12436−12449

AUTHOR INFORMATION

Corresponding Authors

Nicola Taccardi − *Lehrstuhl für Chemische Reaktionstechnik (CRT), Friedrich-Alexander-Universität Erlangen-Nürnberg (FAU), 91058 Erlangen, Germany;* orcid.org/0000-0002-4682-7332; Email: nicola.taccardi@fau.de

Peter Wasserscheid − *Lehrstuhl für Chemische Reaktionstechnik (CRT), Friedrich-Alexander-Universität Erlangen-Nürnberg (FAU), 91058 Erlangen, Germany; Helmholtz-Institute Erlangen-Nürnberg for Renewable Energy (IEK 11), Forschungszentrum Jülich GmbH, 91058 Erlangen, Germany; Institute for a Sustainable Hydrogen Economy, Forschungszentrum Jülich GmbH, 52428 Jülich, Germany;* orcid.org/0000-0003-0413-9539; Email: peter.wasserscheid@fau.de

Authors

Nnamdi Madubuko − *Lehrstuhl für Chemische Reaktionstechnik (CRT), Friedrich-Alexander-Universität Erlangen-Nürnberg (FAU), 91058 Erlangen, Germany*

Tzung-En Hsieh − *Department Interface Design and Energy Materials In-Situ Laboratory Berlin (EMIL), Helmholtz-Zentrum Berlin für Materialien und Energie GmbH (HZB), 12489 Berlin, Germany;* orcid.org/0000-0003-1844-2635

Nora Vorlaufer − *Lehrstuhl für Werkstoffeigenschaften, Friedrich-Alexander-Universität Erlangen-Nürnberg (FAU), 91058 Erlangen, Germany*

Simon Carl − *Lehrstuhl für Werkstoffwissenschaften, Mikro- und Nanostrukturforschung, Friedrich-Alexander-Universität Erlangen-Nürnberg (FAU), 91058 Erlangen, Germany*

Julien Steffen − *Lehrstuhl für Theoretische Chemie, Friedrich-Alexander-Universität Erlangen-Nürnberg (FAU), 91058 Erlangen, Germany; Erlangen National High Performance Computing Center (NHR@FAU), D-91058 Erlangen, Germany;* orcid.org/0000-0001-7933-9557

Andreas Mölkner − *Lehrstuhl für Theoretische Chemie, Friedrich-Alexander-Universität Erlangen-Nürnberg (FAU), 91058 Erlangen, Germany; Erlangen National High Performance Computing Center (NHR@FAU), D-91058 Erlangen, Germany;* orcid.org/0009-0006-3330-5590

Johannes Frisch − *Department Interface Design and Energy Materials In-Situ Laboratory Berlin (EMIL), Helmholtz-Zentrum Berlin für Materialien und Energie GmbH (HZB), 12489 Berlin, Germany*

Regan G. Wilks − *Department Interface Design and Energy Materials In-Situ Laboratory Berlin (EMIL), Helmholtz-Zentrum Berlin für Materialien und Energie GmbH (HZB), 12489 Berlin, Germany;* orcid.org/0000-0001-5822-8399

Johannes Will − *Lehrstuhl für Werkstoffwissenschaften, Mikro- und Nanostrukturforschung, Friedrich-Alexander-Universität Erlangen-Nürnberg (FAU), 91058 Erlangen, Germany;* orcid.org/0000-0003-0326-9913

Marco Haumann − *Lehrstuhl für Chemische Reaktionstechnik (CRT), Friedrich-Alexander-Universität Erlangen-Nürnberg (FAU), 91058 Erlangen, Germany; Research Centre for Synthesis and Catalysis, Department of Chemistry, University of Johannesburg, Auckland Park 2006, South Africa;* orcid.org/0000-0002-3896-365X

Andreas Görling − *Lehrstuhl für Theoretische Chemie, Friedrich-Alexander-Universität Erlangen-Nürnberg (FAU), 91058 Erlangen, Germany; Erlangen National High Performance Computing Center (NHR@FAU), D-91058 Erlangen, Germany;* orcid.org/0000-0002-1831-3318

Erdmann Spiecker − *Lehrstuhl für Werkstoffwissenschaften, Mikro- und Nanostrukturforschung, Friedrich-Alexander-Universität Erlangen-Nürnberg (FAU), 91058 Erlangen, Germany;* orcid.org/0000-0002-2723-5227

Peter Felfer − *Lehrstuhl für Werkstoffeigenschaften, Friedrich-Alexander-Universität Erlangen-Nürnberg (FAU), 91058 Erlangen, Germany*

Marcus Bär − *Department Interface Design and Energy Materials In-Situ Laboratory Berlin (EMIL), Helmholtz-Zentrum Berlin für Materialien und Energie GmbH (HZB), 12489 Berlin, Germany; Department of X-Ray Spectroscopy at Interfaces of Thin Films, Helmholtz Institute Erlangen Nürnberg for Renewable Energy (HI ERN), 12489 Berlin, Germany; Department of Chemistry and Pharmacy, Friedrich-Alexander-Universität Erlangen-Nürnberg (FAU), 91058 Erlangen, Germany;* orcid.org/0000-0001-8581-0691

Complete contact information is available at: https://pubs.acs.org/10.1021/acscatal.5c01463

Author Contributions

N.M., T.H., and N.V. designed and realized the experiments, performed synthesis, characterization, analysis, interpretation, wrote the original draft, reviewed, and edited the final manuscript. S.C. performed HRTEM and HAADF STEM characterization, analysis, interpretation, reviewed, and edited the final manuscript. J.S. and A.M. performed DFT and ML-FF calculations, interpretation, reviewed, and edited the final manuscript. N.T., J.F., R.G.W., and J.W. performed interpretation, reviewed, and edited the final manuscript. M.H., A.G., E.S., P.F., M.B., and P.W. developed the scientific concept, acquired the funding, reviewed, and edited the final manuscript. All authors contributed to the discussion and analysis of the results presented and have given approval to the final version of the manuscript. N.M., T.-E.H., and N.V. contributed equally to this work.

Notes

The authors declare no competing financial interest.

ACKNOWLEDGMENTS

N.M., N.T., M.H., and P.W. thank for financial support by the European Research Council through Project 786475: Engineering of Supported Catalytically Active Liquid Metal Solutions. Additional infrastructural and financial support by the German Research Foundation (DFG) through the collaborative research centers CRC 1452 and CRC1411 is gratefully acknowledged. The authors also gratefully acknowledge the scientific support and HPC resources provided by the Erlangen National High Performance Computing Center (NHR@FAU) of the Friedrich-Alexander-Universität Erlangen-Nürnberg (FAU) under the NHR project b146dc. NHR funding is provided by federal and Bavarian state authorities. NHR@FAU hardware is partially funded by the German Research Foundation (DFG) − 440719683. We thank the Helmholtz-Zentrum Berlin für Materialien und Energie for the allocation of synchrotron radiation beamtime at the SISSY-1 endstation located in the Energy Materials In-situ Laboratory Berlin (EMIL) at the BESSY II synchrotron radiation source. Dr. Mihaela Gorgoi and Dr. Anna Efimenko are gratefully acknowledged for their support in operating the EMIL two-

color beamline during the experimental campaign. EMIL is also acknowledged for making the infrastructure available for the in-system sample preparation and lab-based XPS measurements. Aaron Luke Folkard is gratefully acknowledged for designing the Ga−Pt SCALMS schematic.

REFERENCES

(1) Chen, S.; Chang, X.; Sun, G.; Zhang, T.; Xu, Y.; Wang, Y.; Pei, C.; Gong, J. Propane dehydrogenation: catalyst development, new chemistry, and emerging technologies. *Chem. Soc. Rev.* **2021**, *50*, 3315−3354.
(2) Carter, J. H.; Bere, T.; Pitchers, J. R.; Hewes, D. G.; Vandegehuchte, B. D.; Kiely, C. J.; Taylor, S. H.; Hutchings, G. J. Direct and oxidative dehydrogenation of propane: from catalyst design to industrial application. *Green Chem.* **2021**, *23*, 9747−9799.
(3) Sattler, J. J. H. B.; Ruiz-Martinez, J.; Santillan-Jimenez, E.; Weckhuysen, B. M. Catalytic Dehydrogenation of Light Alkanes on Metals and Metal Oxides. *Chem. Rev.* **2014**, *114*, 10613−10653.
(4) Payard, P. A.; Rochlitz, L.; Searles, K.; Foppa, L.; Leuthold, B.; Safonova, O. V.; Comas-Vives, A.; Copéret, C. Dynamics and Site Isolation: Keys to High Propane Dehydrogenation Performance of Silica-Supported PtGa Nanoparticles. *JACS Au* **2021**, *1*, 1445−1458.
(5) Searles, K.; Chan, K. W.; Mendes Burak, J. A.; Zemlyanov, D.; Safonova, O.; Copéret, C. Highly Productive Propane Dehydrogenation Catalyst Using Silica-Supported Ga−Pt Nanoparticles Generated from Single-Sites. *J. Am. Chem. Soc.* **2018**, *140*, 11674−11679.
(6) Taccardi, N.; Grabau, M.; Debuschewitz, J.; Distaso, M.; Brandl, M.; Hock, R.; Maier, F.; Papp, C.; Erhard, J.; Neiss, C.; Peukert, W.; Görling, A.; Steinrück, H. P.; Wasserscheid, P. Gallium-Rich Pd−Ga Phases as Supported Liquid Metal Catalysts. *Nat. Chem.* **2017**, *9*, 862−867.
(7) Raman, N.; Wolf, M.; Heller, M.; Heene-Würl, N.; Taccardi, N.; Haumann, M.; Felfer, P.; Wasserscheid, P. GaPt Supported Catalytically Active Liquid Metal Solution Catalysis for Propane Dehydrogenation-Support Influence and Coking Studies. *ACS Catal.* **2021**, *11*, 13423−13433.
(8) Hofer, A.; Taccardi, N.; Moritz, M.; Wichmann, C.; Hübner, S.; Drobek, D.; Engelhardt, M.; Papastavrou, G.; Spiecker, E.; Papp, C.; Wasserscheid, P.; Bachmann, J. Preparation of geometrically highly controlled Ga particle arrays on quasi-planar nanostructured surfaces as a SCALMS model system. *RSC Adv.* **2023**, *13*, 4011−4018.
(9) Raman, N.; Maisel, S.; Grabau, M.; Taccardi, N.; Debuschewitz, J.; Wolf, M.; Wittkämper, H.; Bauer, T.; Wu, M.; Haumann, M.; Papp, C.; Görling, A.; Spiecker, E.; Libuda, J.; Steinrück, H.-P.; Wasserscheid, P. Highly Effective Propane Dehydrogenation Using Ga−Rh Supported Catalytically Active Liquid Metal Solutions. *ACS Catal.* **2019**, *9*, 9499−9507.
(10) Wolf, M.; Raman, N.; Taccardi, N.; Haumann, M.; Wasserscheid, P. Coke Formation during Propane Dehydrogenation over Ga−Rh Supported Catalytically Active Liquid Metal Solutions. *ChemCatChem.* **2020**, *12*, 1085−1094.
(11) Wolf, M.; Raman, N.; Taccardi, N.; Horn, R.; Haumann, M.; Wasserscheid, P. Capturing Spatially Resolved Kinetic Data and Coking of Ga−Pt Supported Catalytically Active Liquid Metal Solutions during Propane Dehydrogenation In Situ. *Faraday Discuss.* **2021**, *229*, 359−377.
(12) Zimmermann, T.; Madubuko, N.; Groppe, P.; Raczka, T.; Dünninger, N.; Taccardi, N.; Carl, S.; Apeleo Zubiri, B.; Spiecker, E.; Wasserscheid, P.; Mandel, K.; Haumann, M.; Wintzheimer, S. Supraparticles on beads for supported catalytically active liquid metal solutions − the SCALMS suprabead concept. *Materials Horizons* **2023**, *10*, 4960−4967.
(13) Sebastian, O.; Al-Shaibani, A.; Taccardi, N.; Sultan, U.; Inayat, A.; Vogel, N.; Haumann, M.; Wasserscheid, P. Ga−Pt supported catalytically active liquid metal solutions (SCALMS) prepared by ultrasonication − influence of synthesis conditions on n-heptane dehydrogenation performance. *Catalysis Science & Technology* **2023**, *13*, 4435−4450.
(14) Yan, J.; Lu, Y.; Chen, G.; Yang, M.; Gu, Z. Advances in liquid metals for biomedical applications. *Chem. Soc. Rev.* **2018**, *47*, 2518−2533.
(15) Dickey, M. D. Emerging Applications of Liquid Metals Featuring Surface Oxides. *ACS Appl. Mater. Interfaces* **2014**, *6*, 18369−18379.
(16) Daeneke, T.; Khoshmanesh, K.; Mahmood, N.; de Castro, I. A.; Esrafilzadeh, D.; Barrow, S. J.; Dickey, M. D.; Kalantar-zadeh, K. Liquid Metals: Fundamentals and Applications in Chemistry. *Chem. Soc. Rev.* **2018**, *47*, 4073−4111.
(17) Okamoto, H. Ga-Pt (Gallium-Platinum). *J. Ph. Equilibria Diffus* **2007**, *28*, 494−494.
(18) Hsieh, T.-E.; Maisel, S.; Wittkämper, H.; Frisch, J.; Steffen, J.; Wilks, R. G.; Papp, C.; Görling, A.; Bär, M. Unraveling the Effect of Rh Isolation on Shallow d States of Gallium-Rhodium Alloys. *J. Phys. Chem. C* **2023**, *127*, 20484−20490.
(19) Wittkämper, H.; Hock, R.; Weißer, M.; Dallmann, J.; Vogel, C.; Raman, N.; Taccardi, N.; Haumann, M.; Wasserscheid, P.; Hsieh, T.-E.; Maisel, S.; Moritz, M.; Wichmann, C.; Frisch, J.; Gorgoi, M.; Wilks, R. G.; Bär, M.; Wu, M.; Spiecker, E.; Görling, A.; Unruh, T.; Steinrück, H.-P.; Papp, C. Isolated Rh Atoms in Dehydrogenation Catalysis. *Sci. Rep.* **2023**, *13*, 4458.
(20) Davison, S. G.; Sulston, K. W. Anderson-Newns-Grimley Model. In *Green-Function Theory of Chemisorption*; Davison, S. G.; Sulston, K. W., Eds.; Springer Netherlands: Dordrecht, 2006; pp 45−74.
(21) Newns, D. M. Self-Consistent Model of Hydrogen Chemisorption. *Prhys. Rev.* **1969**, *178*, 1123−1135.
(22) Anderson, P. W. Localized Magnetic States in Metals. *Prhys. Rev.* **1961**, *124*, 41−53.
(23) Nørskov, J. K.; Abild-Pedersen, F.; Studt, F.; Bligaard, T. Density Functional Theory in Surface Chemistry and Catalysis. *Proc. Natl. Acad. Sci. U. S. A.* **2011**, *108*, 937.
(24) Zhang, J.; Vukmirovic, M. B.; Xu, Y.; Mavrikakis, M.; Adzic, R. R. Controlling the Catalytic Activity of Platinum-Monolayer Electrocatalysts for Oxygen Reduction with Different Substrates. *Angew. Chem., Int. Ed.* **2005**, *44*, 2132−2135.
(25) Hammer, B.; Nørskov, J. K. Theoretical surface science and catalysis—calculations and concepts. In *Impact of Surface Science on Catalysis*; Academic Press, 2000; Vol. *45*, pp 71−129.
(26) Nellist, P. D.; Pennycook, S. J. The principles and interpretation of annular dark-field Z-contrast imaging. In *Advances in Imaging and Electron Physics*; Hawkes, P. W., Ed.; Elsevier, 2000; Vol. *113*, pp 147−203.
(27) Wu, M.; Grabau, M.; Taccardi, N.; Papp, C.; Steinrück, H. P.; Wasserscheid, P.; Spiecker, E. Advanced and In-Situ Electron Microscopy Investigation of Phase Composition and Phase Transformation in Ga-Rh Liquid Metal Catalysts. *Microsc. Microanal.* **2019**, *25*, 1878−1879.
(28) Hsieh, T.-E.; Frisch, J.; Wilks, R. G.; Bär, M. Unravelling the Surface Oxidation-Induced Evolution of the Electronic Structure of Gallium. *ACS Appl. Mater. Interfaces* **2023**, *15*, 47725−47732.
(29) Wittkämper, H.; Maisel, S.; Moritz, M.; Grabau, M.; Görling, A.; Steinrück, H. P.; Papp, C. Surface Oxidation-induced Restructuring of Liquid Pd-Ga SCALMS Model Catalysts. *Phys. Chem. Chem. Phys.* **2021**, *23*, 16324−16333.
(30) Carl, S.; Will, J.; Madubuko, N.; Götz, A.; Przybilla, T.; Wu, M.; Raman, N.; Wirth, J.; Taccardi, N.; Zubiri, B. A.; Haumann, M.; Wasserscheid, P.; Spiecker, E. Structural Evolution of GaOx-Shell and Intermetallic Phases in Ga−Pt Supported Catalytically Active Liquid Metal Solutions. *J. Phys. Chem. Lett.* **2024**, *15*, 4711−4720.
(31) Lips, K.; Starr, D. E.; Bär, M.; Schulze, T. F.; Fenske, F.; Christiansen, S.; Krol, R. v. d.; Raoux, S.; Reichardt, G.; Schäfers, F.; Hendel, S.; Follath, R.; Bahrdt, J.; Scheer, M.; Wüstefeld, G.; Kuske, P.; Hävecker, M.; Knop-Gericke, A.; Schlögl, R.; Rech, B. In EMIL: The Energy Materials In Situ Laboratory Berlin, IEEE 40th Photovoltaic Specialist Conference (PVSC), **2014**; p 698.
(32) Grabau, M.; Krick Calderón, S.; Rietzler, F.; Niedermaier, I.; Taccardi, N.; Wasserscheid, P.; Maier, F.; Steinrück, H.-P.; Papp, C.

https://doi.org/10.1021/acscatal.5c01463
ACS Catal. 2025, 15, 12436−12449

Surface Enrichment of Pt in Ga2O3 Films Grown on Liquid Pt/Ga Alloys. *Surf. Sci.* **2016**, *651*, 16−21.
(33) Regan, M. J.; Tostmann, H.; Pershan, P. S.; Magnussen, O. M.; DiMasi, E.; Ocko, B. M.; Deutsch, M. X-ray Study of the Oxidation of Liquid-Gallium Surfaces. *Phys. Rev. B* **1997**, *55*, 10786−10790.
(34) Ohira, S.; Arai, N.; Oshima, T.; Fujita, S. Atomically Controlled Surfaces with Step and Terrace of *β*-Ga2O3 Single Crystal Substrates for Thin Film Growth. *Appl. Surf. Sci.* **2008**, *254*, 7838−7842.
(35) Hsieh, T.-E.; Frisch, J.; Wilks, R. G.; Papp, C.; Bär, M. Impact of Catalysis-Relevant Oxidation and Annealing Treatments on Nanostructured GaRh Alloys. *ACS Appl. Mater. Interfaces* **2024**, *16*, 19858−19865.
(36) Qin, S.; Will, J.; Kim, H.; Denisov, N.; Carl, S.; Spiecker, E.; Schmuki, P. Single Atoms in Photocatalysis: Low Loading Is Good Enough! *ACS Energy Letters* **2023**, *8*, 1209−1214.
(37) Liu, Q.; Zhang, Z. Platinum single-atom catalysts: a comparative review towards effective characterization. *Catalysis Science & Technology* **2019**, *9*, 4821−4834.
(38) Vorlaufer, N.; Josten, J.; Carl, S.; Göbel, E.; Søgaard, A.; Taccardi, N.; Spiecker, E.; Felfer, P. Preparation of atom probe tips from (nano)particles in dispersion using (di)electrophoresis and electroplating. *Microsc. Res. Tech.* **2023**, *87*, 476−483.
(39) Cussler, E. L. *Diffusion: Mass Transfer in Fluid Systems*, 3rd ed.; Cambridge University Press: Cambridge, 2009.
(40) Catalán-Gómez, S.; Redondo-Cubero, A.; Morales, M.; de la Mata, M.; Molina, S. I.; Palomares, F. J.; Carnicero, A.; Pau, J. L.; Vázquez, L. Modification of the Mechanical Properties of Core-Shell Liquid Gallium Nanoparticles by Thermal Oxidation at Low Temperature. *Part. Part. Syst. Charact.* **2021**, *38*, No. 2100141.
(41) Rosseau, L. R. S.; Medrano, J. A.; Bhardwaj, R.; Goetheer, E. L. V.; Filot, I. A. W.; Gallucci, F.; van Sint Annaland, M. On the Potential of Gallium- and Indium-Based Liquid Metal Membranes for Hydrogen Separation. *Membranes* **2022**, *12*, 75.
(42) Deveau, N. D.; Yen, P.-S.; Datta, R. Evaluation of hydrogen sorption and permeation parameters in liquid metal membranes via Sieverts' apparatus. *Int. J. Hydrogen Energy* **2018**, *43*, 19075−19090.
(43) Mazayev, S. N.; Prokofiev, Y. G. Hydrogen inventory in gallium. *J. Nucl. Mater.* **1994**, *212−215*, 1497−1498.
(44) Raman, N.; Söllner, J.; Madubuko, N.; Nair, S.; Taccardi, N.; Thommes, M.; Haumann, M.; Wasserscheid, P. Top-down vs. bottom-up synthesis of Ga−based supported catalytically active liquid metal solutions (SCALMS) for the dehydrogenation of isobutane. *Chem. Eng. J.* **2023**, *475*, No. 146081.
(45) Cybulskis, V. J.; Pradhan, S. U.; Lovón-Quintana, J. J.; Hock, A. S.; Hu, B.; Zhang, G.; Delgass, W. N.; Ribeiro, F. H.; Miller, J. T. The Nature of the Isolated Gallium Active Center for Propane Dehydrogenation on Ga/SiO2. *Catal. Lett.* **2017**, *147*, 1252−1262.
(46) Takahara, I.; Saito, M.; Inaba, M.; Murata, K. Effects of Pre-Treatment of a Silica-Supported Gallium Oxide Catalyst with H2 on Its Catalytic Performance for Dehydrogenation of Propane. *Catal. Lett.* **2004**, *96*, 29−32.
(47) Samanta, A.; Bai, X.; Robinson, B.; Chen, H.; Hu, J. Conversion of Light Alkane to Value-Added Chemicals over ZSM-5/Metal Promoted Catalysts. *Ind. Eng. Chem. Res.* **2017**, *56*, 11006−11012.
(48) Shpiro, E. S.; Shevchenko, D. P.; Tkachenko, O. P.; Dmitriev, R. V. Platinum promoting effects in Pt/Ga zeolite Catalysts of lower alkane aromatization. I. Ga and Pt electronic states, dispersion and distribution in zeolite crystals in dependence of preparation techniques. Dynamic effects caused by reaction mixture. *Applied Catalysis A: General* **1994**, *107*, 147−164.
(49) Caiola, A.; Robinson, B.; Bai, X.; Shekhawat, D.; Hu, J. Study of the Hydrogen Pretreatment of Gallium and Platinum Promoted ZSM-5 for the Ethane Dehydroaromatization Reaction. *Ind. Eng. Chem. Res.* **2021**, *60*, 11421−11431.
(50) Nair, S.; Coca-Lopez, N.; Madubuko, N.; Portela, R.; Taccardi, N.; Haumann, M.; Bañares, M. A.; Wasserscheid, P. In Situ Raman Spectroscopy of Supported Catalytically Active Liquid Metal Solutions (SCALMS)—Activation and Coking Behavior in Propane Dehydrogenation. *ChemCatChem* **2025**, No. e202500176.
(51) Hohner, C.; Kettner, M.; Stumm, C.; Blaumeiser, D.; Wittkämper, H.; Grabau, M.; Schwarz, M.; Schuschke, C.; Lykhach, Y.; Papp, C.; Steinrück, H.-P.; Libuda, J. Pt−Ga Model SCALMS on Modified HOPG: Thermal Behavior and Stability in UHV and under Near-Ambient Conditions. *J. Phys. Chem. C* **2020**, *124*, 2562−2573.

https://doi.org/10.1021/acscatal.5c01463
ACS Catal. 2025, 15, 12436−12449